Green Sciences
Volume 28 Issue 1 · pp. 115–131 · DOI: 10.2478/pjct-2026-0009

Development and characterization of CO_2 micro-nano dispersion system for enhanced oil recovery from shale oil

Research Article

Tao Zhang[1], Bengang Li[1], Baoche Liu[1], Tenghuan Zhang[1], Jianke Ren[1], Chunmei Xu[1], Shijun Chen[2]*

[1] *Oil and Gas Technology Institute, PetroChina Changqing Oilfield Company, Xi 'an 710018, China*
[2] *College of Chemistry and Chemical Engineering, Xi'an SHIYOU University, Xi'an, 710065, China*

Received 30 July 2025; Accepted 11 December 2025

Abstract: This study examines the characteristics of strong heterogeneity, low porosity, and low permeability in shale oil reservoirs and develops a CO_2 micro-nano dispersion system designed to enhance shale oil recovery. CO_2 nano bubbles were prepared by hydraulic cavitation. Experimental results showed that CO_2 nano bubbles exhibited good relative stability in deionized water for a short period but were significantly affected by the Ostwald ripening effect over a longer period. The study found that inorganic salts and surfactants had significant regulatory effects on bubble size and relative stability, with nonionic surfactants exhibiting the best stabilizing effect through a steric hindrance mechanism. The stimulation experiment indicated that the recovery rate of the CO_2/low-salinity water/surfactant composite system was significantly higher than that of single CO_2 injection, and injection pressure, gas–liquid ratio, and injection rate had important impacts on oil displacement.

Keywords: *CO_2 stimulation • Inorganic salt • Micro-nano bubbles • Shale oil reservoir • Surfactant*

1. Introduction

Shale oil reservoirs are characterized by strong heterogeneity, poor reservoir physical properties, significant differences in pore throats, low porosity, low permeability, high original viscosity, poor fluidity, and strong capillary force effects within nano-pores [1]. Shale oil is mainly stored in storage spaces such as micro-fractures and nano-pores in free and adsorbed states. CO_2 injection and stimulation [2,3], low-salinity water (LSW) flooding, and surfactant spontaneous imbibition [4,5] are currently key technologies for enhancing the recovery rate of shale oil reservoirs. Among them, gas injection stimulation utilizes the strong diffusivity of small molecules such as CO_2 to supplement formation energy. Under high-pressure conditions, it is easier for CO_2 to enter shale nano-pores through diffusion and displace crude oil. Furthermore, the nano-confined effect can significantly reduce the miscibility pressure between CO_2 and crude oil. Research has shown that CO_2 stimulation is highly suitable for the development of low-permeability shale oil reservoirs. However, the application of this technology also faces significant challenges. On the one hand, limited by the structure of shale nano-pores, the diffusion rate of CO_2 molecules is slow, and the injected CO_2 mainly remains in the fracture system, making it difficult to effectively penetrate the matrix. This leads to severe gas channeling in the field and poor development results. On the other hand, due to the low critical parameters of CO_2 (31.1°C, 7.38 MPa), it often exists in a supercritical state under reservoir conditions [6,7]. Although it has advantages such as fast diffusion, high density, and low viscosity, the presence of the fracture system causes the continuously injected CO_2 to preferentially flow along high-permeability channels, significantly reducing effective contact with matrix crude oil. For the issue of gas channeling, although the CO_2/brine alternating injection and foam flooding techniques used in conventional reservoirs have achieved certain results, the particularities of

* *E-mail: csj19792018@sina.com*

shale oil reservoirs make traditional foam stabilizers difficult to function. Therefore, the emerging CO_2 microbubble flooding technology [8,9] in recent years provides a new approach for improving the CO_2 flooding effect in shale oil reservoirs by enhancing CO_2 solubility and mass transfer efficiency.

Micro-nano bubbles [10–12] are emerging as a promising new green enhancement technology in the field of shale oil reservoir development, owing to their unique physicochemical properties, including ultra-large specific surface area, slow rising speed, high mass transfer efficiency, and surface charge characteristics. Compared to traditional bubbles, these characteristics exhibit significant advantages in improving CO_2 utilization efficiency, providing an innovative solution for the efficient development of shale oil resources. Furthermore, inorganic salts and surfactants, as key components regulating the relative stability of nano-bubbles, simultaneously possess the dual function of promoting spontaneous imbibition and oil displacement. Based on these characteristics, by constructing a micro-nano gas–liquid dispersion system with CO_2 as the dispersed phase and a low-salinity surfactant solution as the continuous phase, it is expected to develop into a new technology with great application prospects for efficient shale oil development. Xue et al. [13] experimentally confirmed that the use of CO_2 micro-bubble injection technology can increase the dissolution rate of gas in the formation by 20% compared to conventional CO_2 injection. This injection method can significantly reduce the occurrence of free CO_2 in the reservoir, which not only helps to improve crude oil recovery but also enhances the long-term relative stability of CO_2 geological storage. Guo et al. [14] found in their study on the influence of inorganic salts on micro-nano bubbles that ionic valence is a key parameter regulating bubble size distribution and zeta potential evolution, and trivalent cations can quickly adsorb to the bubble interface, significantly increasing the interface zeta potential to a positive value. In addition, as the electrolyte concentration increases, resulting in enhanced ionic strength, it triggers a synergistic change in the average particle size of nano-bubbles and a decrease in zeta potential. Jadhav et al. [15] studied the influence of surfactants on micro-nano bubbles and found that anionic surfactants carry the same charge as the surface of micro-nano bubbles, making it difficult for them to adsorb at the bubble interface due to electrostatic repulsion. However, when the van der Waals attraction between the two is strong enough, it can overcome the electrostatic barrier to achieve surface adsorption. Zhou's research [16] showed that changes in the adsorption concentration of nonionic surfactant molecules and the synergistic effect of the gas–liquid interface of nano-bubbles are key factors determining the surface tension of nano-bubbles. Rong et al. [17] used the lattice Boltzmann method to numerically simulate the flow behavior of CO_2 micro-bubbles in formation water. Their simulation results indicated that the size distribution of micro-bubbles is mainly regulated by two key factors: the physicochemical properties of formation fluid and the CO_2 injection rate. The research reveals the dynamics of negative correlation – as the injection rate decreases, the system generates smaller-sized CO_2 microbubbles.

With deepening understanding of the characteristics and mechanisms of micro-nano bubbles, this emerging technology demonstrates unique advantages in CO_2 enhanced oil recovery (CO_2-EOR) and carbon sequestration applications. It is expected to become a revolutionary solution that is both economical and environmentally friendly. Therefore, it is necessary to further develop a CO_2 micro-nano dispersed composite flooding system with bubble sizes in the micro-nano range and good dispersion relative stability, targeting the characteristics of shale oil reservoirs and development, to provide technical reserves for the efficient development of shale oil and gas resources.

2. Materials and methods

2.1 Materials

The chemical raw materials used in the experiment include sodium hydroxide, hydrogen chloride, carbon dioxide, and deionized water. Among them, sodium hydroxide and hydrogen chloride are of analytical reagent (AR) grade, purchased from Shanghai Macklin Biochemical Technology Co., Ltd. Carbon dioxide was of AR grade, supplied by Beijing Qianxi Jingcheng Gas Co., Ltd. Deionized water was self-made in the laboratory.

2.2 Apparatus

The instruments and equipment used in this experiment are as follows: An AL104 electronic balance manufactured by Mettler-Toledo Instruments (Shanghai) Co., Ltd was employed for weighing purposes. Stirring equipment included a JB-1 magnetic stirring device from Shanghai Leici Chuangyi Instrumentation Co., Ltd and a GZ-120WS mechanical stirring device supplied by Shanghai Pingxuan Scientific Instrument Co., Ltd. A PHS-3E portable pH meter produced by Shanghai INESA Scientific Instrument Co., Ltd was used for pH measurement. A DHG electric forced-air

drying oven from Shanghai Yiheng Scientific Instrument Co., Ltd was utilized for drying treatment. The particle size and surface charge characteristics of nano bubbles were characterized by a 90 Plus PALS nanoparticle size and zeta potential analyzer from Brookhaven Instruments, Inc. (USA), while the particle concentration and distribution were determined using a NanoSight NS300 nanoparticle tracking analyzer from Malvern Panalytical Ltd. (UK). The preparation of CO_2 micro-nano bubbles was conducted with a ZCJ-NM micro-nano bubble generator manufactured by Shanghai Zhongjing Environmental Protection Technology Co., Ltd.

2.3 Method for generating CO_2 nano bubbles

In this study, a commercial nano bubble generation device based on the principle of hydrodynamic cavitation was employed to prepare CO_2 nano bubbles (Figure 1). The experimental system consisted of a high-pressure CO_2 gas source, a nano bubble generation host, and a 2 L glass receiving container. The generator was equipped with a digital control panel, allowing precise adjustment of gas–liquid circulation time (0–100 min) and gas flow rate (0–200 mL/min). Its working principle involved generating negative pressure vortices through a rotor system, subjecting the mixed fluid of CO_2 (or N_2) and deionized water (self-made in the laboratory, conductivity 0.085 μS/cm) to high-speed shear at the membrane dispersion component, and inducing gas heterogeneous nucleation through dynamic pressure changes at the gas–liquid interface, ultimately forming nanoscale CO_2 bubbles. Prior to the experiment, all contact surfaces were cleaned with deionized water and analytical-grade ethanol for 3–5 times, and plastic baffles were used to seal the reaction container during testing to ensure the system was protected from environmental contaminants.

2.4 Characterization and testing

The average size, dispersibility, and number concentration of bubbles are key parameters for understanding the basic characteristics of nano bubbles [18,19]. The

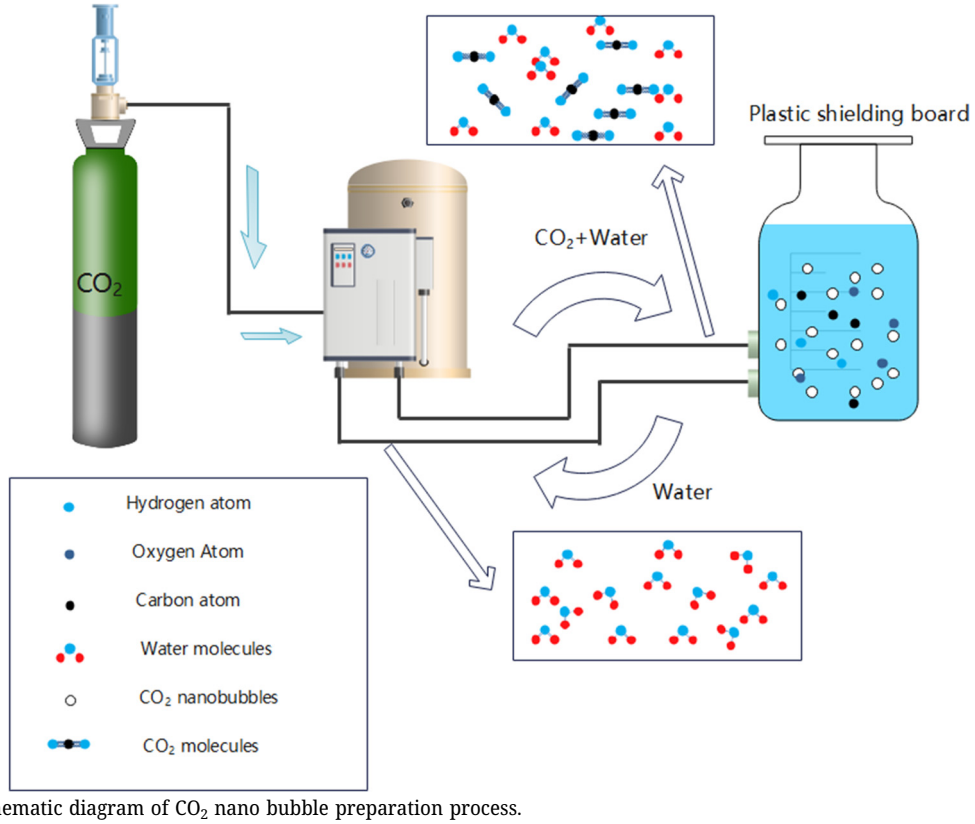

Figure 1. Schematic diagram of CO_2 nano bubble preparation process.

dispersion coefficient δ and average count rate (ACR) values obtained through cumulative distribution analysis via dynamic light scattering (DLS) and nanoparticle tracking analysis enable precise measurement of bubble dispersion and number concentration [20,21]. Therefore, the characterization of CO_2 micro and nano bubbles focuses on studying the changes in the average size, dispersibility coefficient δ (assessing the uniformity and stability of the dispersed phase's distribution within the dispersion medium), and ACR values of bubbles with standing time.

2.4.1 Relative stability characterization of CO_2 nano bubbles

Average size, dispersity, and number concentration are core parameters for characterizing the basic properties of CO_2 nano bubbles [18,19]. This study took pH = 7.0 as the set condition, and systematically carried out the relative stability (nanobubbles can maintain the nanoscale instead of rapidly coalescing into micro/milliscale bubbles) within a certain duration, and whether the attenuation rate of core characteristics (e.g., particle size, number concentration) matches application-oriented requirements. Characterization experiment of CO_2 nano bubbles is carried out in two working conditions: static and flow.

In the static condition test, a CO_2 nano bubble dispersion system with an average particle size of approximately 400 nm was first prepared using the basic parameters of 6 min gas–liquid circulation time and 150 mL/min gas flow rate. Meanwhile, a pH gradient experiment was added, and the same system was prepared synchronously under different pH conditions (1.5, 3.0…9.0, 10.5). Subsequently, the average bubble diameter and polydispersity index (PDI) were obtained via DLS (cumulative method), while the number concentration was measured by nanoparticle tracking analysis (NTA). The ACR from DLS functions exclusively as a relative indicator of the instrument's scattered signal intensity, and it is not utilized for number concentration conversion [20,21].

To address the flow relative stability issue of nano bubbles in industrial scenarios, a 0–60 min circulating flow experiment was further designed, with two comparative conditions of 10 mL/min (low flow rate) and 20 mL/min (high flow rate). Similarly, a nanoparticle size and zeta potential analyzer was used to explore the dynamic effects of different flow rates on the CO_2 nano bubble system.

2.4.2 Relative stability characterization of CO_2 nano bubbles under the influence of external factors

This section investigates the regulatory mechanisms of inorganic salts and surfactants on CO_2 nano bubble relative stability. For inorganic salt experiments, NaCl and $CaCl_2$ (0.1–1.0 mol/L) were used. After preparation following Section 2.3, DLS and zeta potential methods from Section 2.4.1 were applied to determine particle size distribution, surface charge, and 0–70 h particle size changes, comparing the electric double layer screening effect differences between Na^+ and Ca^{2+}. Surfactant experiments covered anionic (α-olefin sulfonate [AOS]), cationic (cetyltrimethylammonium bromide [CTAB]), and nonionic (dodecyl/tetradecyl glucoside [APG] and nonylphenol polyoxyethylene ether [NP40]) types with concentrations of 0.1–1 wt% (or 0.01–0.5 critical micelle concentration [CMC]). Through the same preparation and characterization procedures, combined with particle size evolution data, the differences in regulatory mechanisms via interfacial charge or surface tension were analyzed.

2.4.3 Huff-Puff test of CO_2 micro-nano system

This test employed a core displacement device and nanoparticle tracking analyzer to systematically investigate the huff-puff imbibition effects of three systems: pure CO_2 system, CO_2 + LSW-50 binary system, and CO_2 + LSW-50 + nonionic surfactant NP40 (concentrations of 0.01/0.1/0.5 wt%) ternary system. By regulating key parameters such as pressure, gas–liquid ratio, and injection rate, the influence of different experimental conditions on the displacement efficiency of the systems was examined.

3. Results and discussion

3.1 Study on characteristics of CO_2 nano bubbles prepared by hydrodynamic cavitation

Hydrodynamic cavitation has become a mainstream technology for micro-nano bubble preparation due to its advantages of simple operation, strong scalability, and commercial viability, demonstrating significant application value in petroleum industry processes such as crude oil upgrading and EOR [8,22,23]. This chapter prepares surfactant-free CO_2 nano bubbles using this method. Targeting the characteristic of shale oil reservoirs that primarily store oil in nano-scale pores (mostly <50 nm in diameter with poor connectivity) [1], the study systematically characterizes key parameters including size distribution, number concentration, and zeta potential under static and dynamic conditions to reveal the dynamic evolution law of nano bubbles, providing experimental basis

for relative stability optimization of CO_2 micro-nano dispersion systems in industrial scenarios. As a core prerequisite for effective shale oil development, the injectability and relative stability of CO_2 micro-nano dispersions highly depend on the characteristic performance of bubbles in complex pore environments. By comparing and analyzing bubble characteristic parameters under static and dynamic conditions, this research can provide critical data for clarifying their migration mechanism in shale pores, which is of great guiding significance for promoting the practical application of this technology [5].

3.1.1 Basic characteristics and relative stability of CO_2 nano bubbles under static conditions

Under the experimental conditions of a gas–liquid circulation time of 6 min and a gas flow rate of 150 mL/min, a CO_2 nano bubble dispersion system with an initial average particle size of approximately 177 nm was successfully prepared (Figure 2a). As shown in Figure 2, the research system investigated the evolution of particle size of the CO_2 nano bubble system over a period of 0–75 h, while simultaneously monitoring the dynamic changes in the dispersibility coefficient δ and the ACR.

This study systematically reveals the relative stability regulation law and mechanism of CO_2 nano bubbles: As shown in Figure 2c, CO_2 nano bubbles exhibit a two-stage evolution of "slow growth-fast coarsening" in deionized water: in the first 20 h, the particle size increases from ~450 nm to 560 nm (24% increase) due to CO_2's high water solubility buffering the mass transfer rate of Ostwald ripening. After 20 h, liquid-phase CO_2 becomes saturated, and Ostwald ripening plus Brownian motion-induced coalescence jointly drive rapid coarsening, reaching ~900 nm at 75 h. In contrast, N_2 nano bubbles increase from 350 to 600 nm within 75 h without obvious two-stage behavior (as N_2 has extremely low water solubility, and its evolution relies more on simple coalescence and ripening). CO_2's high solubility regulates the evolution rhythm via "dissolution-saturation," making its timeliness more staged [24]. In Figure 2b, the average size of CO_2 nano bubbles shows a sinusoidal change in "increase → decrease → slow increase" with temperature, resulting from the competition between the "coalescence effect of Ostwald ripening" and the "bubble

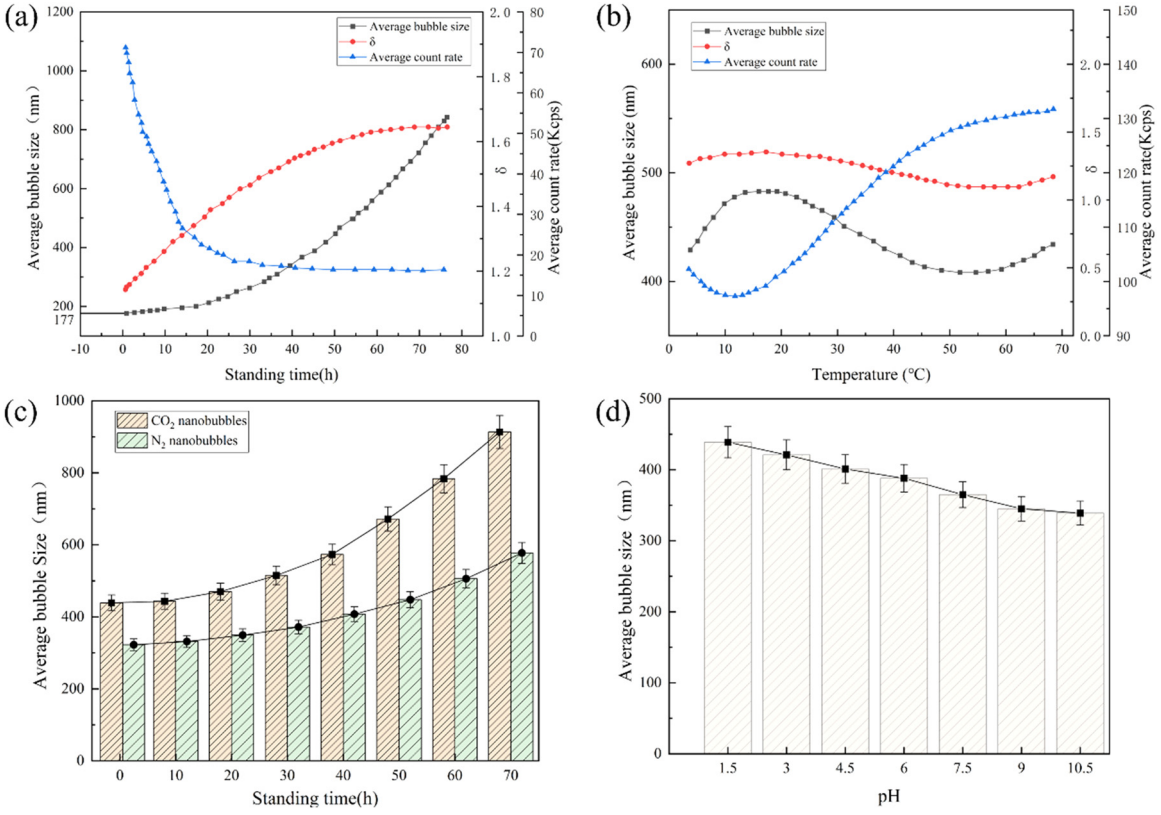

Figure 2. Size change characteristics of CO_2 nano bubbles under static conditions. (a) Effect of standing time; (b) effect of temperature; (c) effect of gas type; (d) effect of pH.

shrinking effect regulated by CO_2 solubility": the coalescence effect dominates size growth at 5–20°C. The "shrinking effect" dominates size decrease between 20 and 50°C (40°C is the critical balance point of the two effects) as CO_2 solubility decreases with rising temperature. Above 50°C, the shrinking effect moderates and the coalescence effect dominates again, causing slow size increase. The high solubility of CO_2 (1.45 g/kg) amplifies the "solubility-temperature" regulation on size, making it exhibit this unique law (due to low solubility, N_2 nano bubbles rely more on thermal motion-induced coalescence for size change without the intermediate decreasing stage) [25]. The pH regulation experiment found that hundreds of nanometer-sized bubbles can be formed in a wide range from acidic to alkaline (pH 2–12), but under alkaline conditions, they exhibit significantly enhanced relative stability (Figure 2d). On the one hand, based on the experimental results regarding temporal evolution (two-stage "dissolution-saturation buffering"), temperature response (40°C effect balance threshold), and pH adaptation (enhanced charge repulsion under alkaline conditions), these findings clearly elucidate the relative stability mechanism of CO_2 nano bubbles, which centers on "mass transfer buffering mediated by high water solubility + synergistic regulation of interfacial charges." On the other hand, the revealed temperature control threshold (40°C), pH adaptation range (2–12, with better performance under alkaline conditions), and temporal evolution law provide a quantitative basis for the parameter optimization of CO_2 nano bubble systems in oil and gas extraction (e.g., control of injection temperature, adjustment of reservoir pH adaptation). Particularly for alkaline reservoirs, these findings can directly guide the stability design of injection systems, significantly enhancing the application adaptability and effectiveness of this technology in practical extraction scenarios.

The zeta potential of CO_2 nano bubbles exhibits a notable relative stability decay characteristic over time (Figure 3). Experimental data reveal that within the initial 9 h, the zeta potential remains stable within the range of −18 to −21 mV, indicating good short-term relative stability of the bubble system. However, when the standing time is extended to 24–72 h, the absolute value of the potential decreases significantly, and it is already below 10 mV at 72 h. This potential decay phenomenon originates from changes in the charge characteristics at the gas–liquid interface: due to the significant thermodynamic potential difference between OH^- (adsorption energy −446.8 kJ/mol) generated by water molecule ionization and H^+ (−1,104 kJ/mol), OH^- preferentially adsorbs onto the bubble surface, forming a negative charge layer. Over time, this surface charge gradually dissipates, weakening the electrostatic repulsion force and ultimately promoting bubble coalescence. Based on the kinetic analysis of potential decay, it is once again verified that the effective stable time of CO_2 nano bubbles under static conditions is approximately 72 h. This discovery provides important time-dependent parameters for the practical application of nano bubble systems.

3.1.2 Basic characteristics and relative stability of CO_2 nano-bubbles in a flowing state

In practical applications, nano bubbles are often found in complex flow environments. Therefore, focusing on the relative stability of nano bubbles in industrial flow

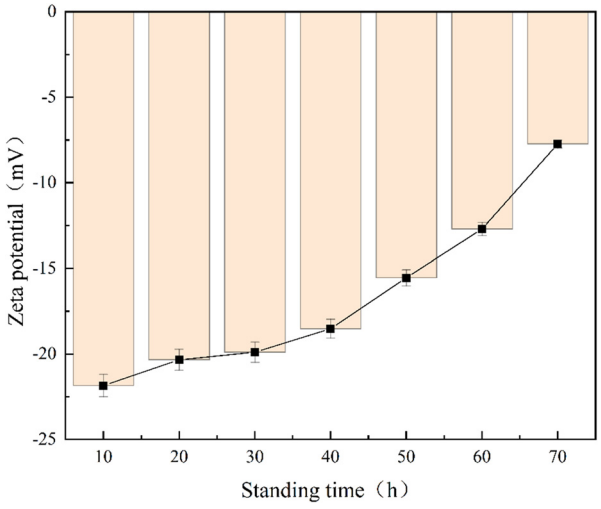

Figure 3. Characteristics of zeta potential changes in CO_2 nano bubbles under static conditions.

environments, we systematically investigated the dynamic effects of different flow rates on the CO_2 nano bubble system under flowing conditions. By designing a cyclic flow experiment (0–60 min), we compared and analyzed the particle size evolution and zeta potential changes in CO_2 nano bubbles under low flow rate (10 mL/min) and high flow rate (20 mL/min) conditions. This revealed the regulation mechanism of fluid shear action on nano bubble relative stability, providing an experimental basis for the optimal control of nano bubble parameters in industrial applications.

Figure 4 reveals the dynamic evolution characteristics of CO_2 nano bubbles under different flow rates. Experimental data in Figure 4a shows that during the cyclic flow process from 0 to 60 min, the average size of the bubbles increases significantly with the increase in flow rate: the particle size fluctuates within the range of 480–930 nm under low-speed conditions (10 mL/min), while it increases to 700–1,500 nm under high-speed conditions (20 mL/min). The study found that the flow process exhibits a typical "disturbance-equilibrium" dynamic mechanism: in the initial stage, the energy input from the micro-nano bubble generator breaks the gas–liquid dynamic equilibrium and enhances bubble collisions. Subsequently, the system gradually tends toward a new dynamic equilibrium. It is worth noting that the increase in flow rate not only increases the maximum particle size by 35% but also extends the dynamic equilibrium establishment time by about 50%.

Experimental data in Figure 4b and c reveal the multiple impacts of flow conditions on the CO_2 nano bubble system: First, the bubble size dispersibility coefficient (δ value) gradually increases with increasing flow rate. Second, dynamic flow enables the bubble concentration to be stably maintained at a relatively high level (90–110 Kcps), which is more than half as high as that under static conditions. This is primarily attributed to the continuous

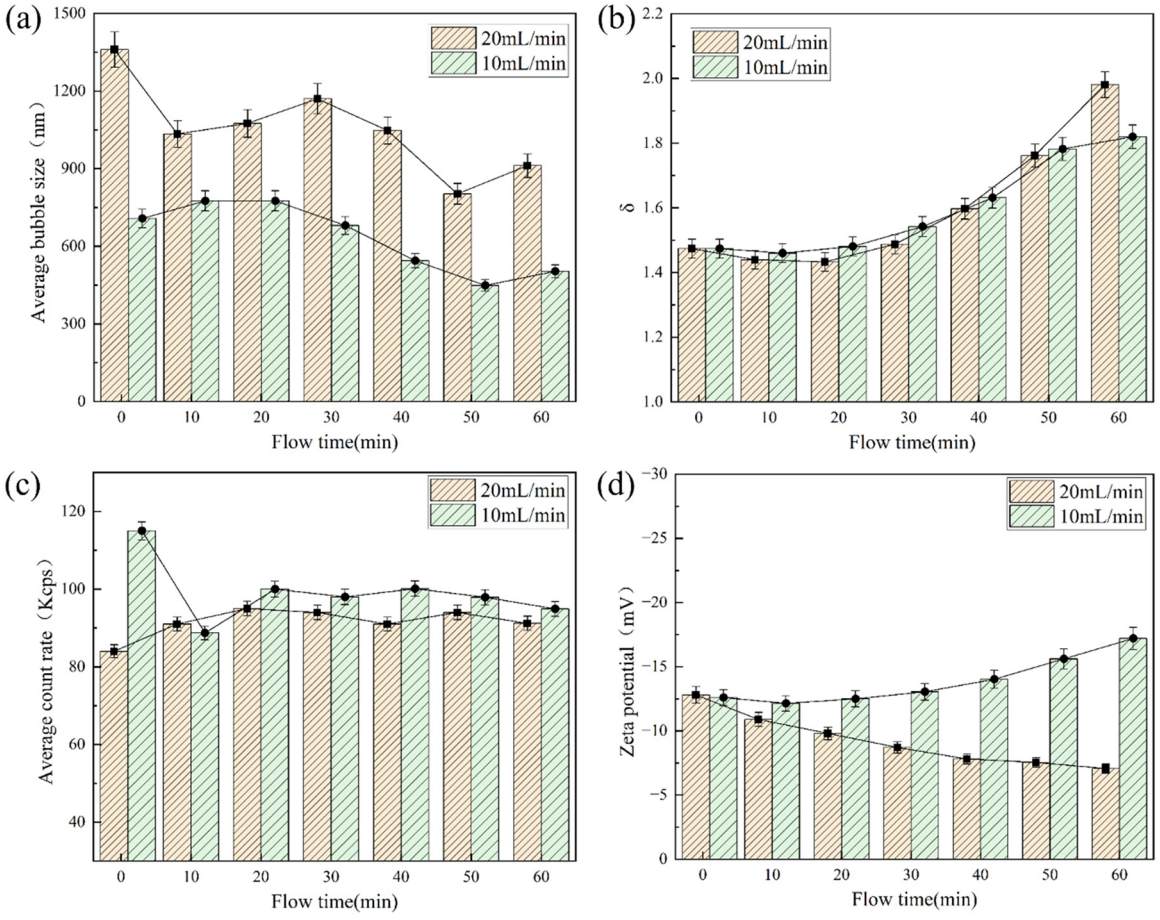

Figure 4. Characteristics of changes in average size and zeta potential of CO_2 nano bubbles under flow mode. (a) Result of bubble size; (b) result of dispersibility coefficient; (c) result of count rate; (d) result of zeta potentia.

energy input from the micro-nano bubble generator, promoting the processes of bubble formation and regeneration. This high concentration state, in turn, accelerates the dynamics of bubble coalescence, ultimately leading to the formation of larger bubbles. This study quantifies for the first time the coupled mechanism of "high concentration-wide distribution-low relative stability" in industrial flow systems, providing key insights for parameter optimization in practical applications.

Figure 4d reveals the regulation of flow rate on the surface potential of CO_2 nano bubbles. The study shows that under dynamic flow conditions (0–60 min), the potential of CO_2 nano bubbles exhibits significant flow rate dependence: when the flow rate is <10 mL/min, the potential stabilizes at −20 to −15 mV. However, when the flow rate is increased to 20 mL/min, the absolute value of the potential gradually approaches 0 mV. This potential decay phenomenon stems from a dual mechanism: on the one hand, high-speed flow promotes bubble collision and coalescence, leading to an increase in particle size (consistent with the sudden potential change rule of micro-nano bubbles discovered by Pan et al. [26]). On the other hand, the flow shear effect disrupts the double-layer structure, causing surface charges to redistribute. Especially when the bubble radius exceeds 1 μm, changes in the ion concentration distribution at the interface significantly reduce the absolute value of the potential.

DLS and zeta potential measurements indicate that the formation of CO_2 nano bubbles is a dynamic process, with their size and surface charge evolving continuously over time (Figure 5). Under static conditions, the supersaturated CO_2 solution initially forms nanoscale gas clusters (several nanometers) that are stabilized by surface energy and charge interactions. As the gas saturation decreases, these clusters gradually grow into nano bubbles. Due to Brownian motion and weak buoyancy forces, nano bubbles can remain suspended for a long time, but they can coalesce to form larger bubbles and eventually burst. In a flowing state, bubble behavior is regulated by fluid dynamics: at low flow rates, nano bubbles move stably with laminar flow. Increased flow rates intensify bubble collisions, leading to a broader size distribution, but continuous energy input maintains a high bubble concentration. This evolutionary mechanism confirms previous research findings that the essence of nano bubbles is dynamic gas clusters [27].

3.2 Analysis of the influence of external factors on the relative stability of CO_2 nano bubbles

When constructing CO_2 micro-nano dispersion systems, inorganic salts and surfactants not only act as continuous phases to exert spontaneous imbibition and oil displacement, but also contain salt ions and surfactant molecules that directly affect the generation and relative stability characteristics of CO_2 nano bubbles (Figure 6). Therefore, it is necessary to further clarify the interaction mechanism between salt ions and surfactants, and CO_2 nano bubbles. This study systematically investigated the synergistic effect mechanism of inorganic salt ions and surfactant molecules on the generation and relative stability characteristics of CO_2 nano bubbles by regulating the concentration gradient of NaCl and $CaCl_2$ solutions (0.1–1.0 mol/L) and four surfactants (0.1–1 wt%), providing a theoretical basis for constructing CO_2 micro-nano dispersion systems with good dispersion relative stability.

3.2.1 Impact of inorganic salts on CO_2 nano bubbles

(1) The influence of salt ions on the relative stability of CO_2 nano bubbles

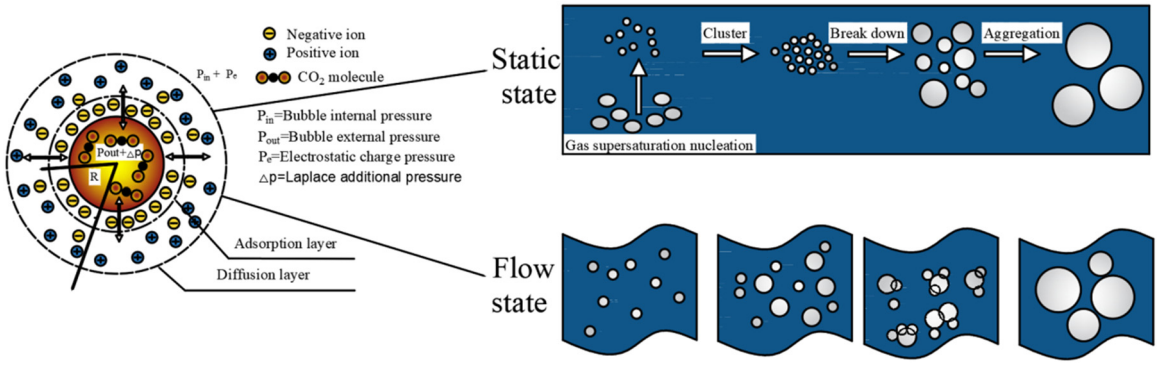

Figure 5. Evolution process of CO_2 nano bubbles with time under static and flowing conditions.

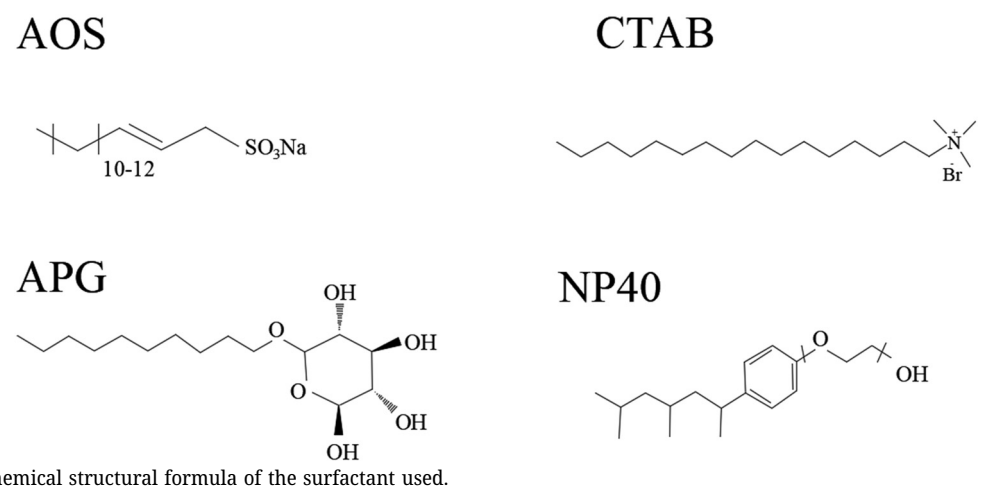

Figure 6. Chemical structural formula of the surfactant used.

Figure 7 reveals the regulatory mechanism of electrolytes on the physicochemical properties of CO_2 nano bubbles. Experimental data show that: (1) In terms of particle size evolution, salt ions significantly increase the average size of bubbles. 0.01 wt% NaCl and $CaCl_2$, respectively, increases the particle size from 400 nm to 468 nm and 504 nm, and the growth-promoting effect of divalent Ca^{2+} is 35% stronger than that of Na^+. (2) In terms of surface potential, salt ions cause a decrease in the absolute value of zeta potential, and 0.1 wt% $CaCl_2$ even triggers charge reversal (negative → positive), which is due to the charge neutralization effect between high valence ions and interface OH^-.

(2) Changes in CO_2 nano bubbles formed by different types and concentrations of salt particles over time

From the analysis of Figure 8, it can be seen that salt ions accelerate the process of bubble coarsening. The system containing 0.01 wt% NaCl shows a 100% increase in particle size (400–800 nm) within 70 h, while the same concentration of $CaCl_2$ system only takes 20 h to reach 1μm. In addition, the coarsening rate of Ca^{2+} system is faster than that of Na^+, which is directly related to the stronger charge neutralization ability of divalent ions.

3.2.2 Influence of surfactants on CO_2 nano bubbles

(1) The influence of surfactant type and concentration on the size distribution of CO_2 nano bubbles

This study selected four types of surfactants: anionic AOS (α-olefin sulfonate), cationic CTAB (cetyltrimethylammonium

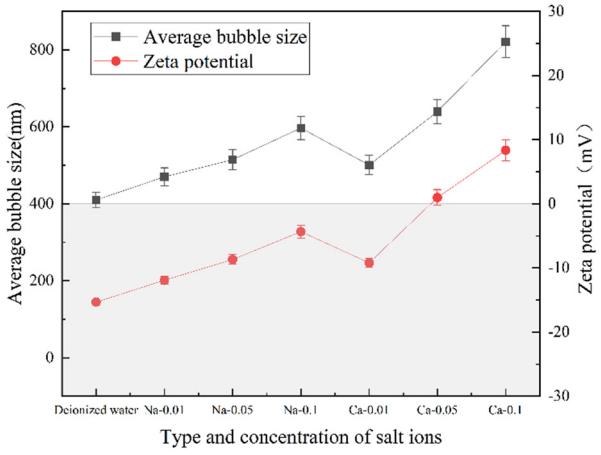

Figure 7. The influence of salt ions on the relative stability of CO_2 nano bubbles.

bromide), nonionic APG-1214 (dodecyl/tetradecyl glucoside), and nonionic NP40 (nonylphenol polyoxyethylene ether). Before the generation of CO_2 nanobubbles, they were formulated into 0.1–1 wt% aqueous solutions, and then introduced into a hydraulic cavitation generator together with CO_2 to prepare bubbles, ensuring that the surfactants participate in the formation and stabilization of bubbles throughout the process. The basic properties of the four surfactants are as follows: AOS has a molecular weight of 300–400 g/mol, a CMC of 0.01–0.05 mmol/L, and molecules carry negative charges ($–SO_3^-Na^+$). CTAB has a molecular weight of 364.45 g/mol, a CMC of 0.9–1.1 mmol/L, and molecules carry positive charges ($–N^+(CH_3)_3Br^-$). APG-1214 has a molecular weight of 480–550 g/mol, a CMC of 0.05–0.1 mmol/L, and molecules are electrically neutral. NP40 has a molecular weight of 600–700 g/mol, a CMC of 0.02–0.04 mmol/L, and molecules are electrically neutral. Based on the analysis of Figure 9 (where Figure 9a–d correspond to the particle size distributions of AOS, CTAB, APG-1214, and NP40 systems, respectively), the regulation of surfactants on the size distribution of CO_2 nanobubbles shows significant concentration and type dependence: when the concentration increases from 0.01 CMC to 0.5 CMC, the particle size distribution peaks of the four systems all shift to smaller sizes and the peak widths narrow, with an overall decrease of 60% in the average particle size (due to the increased concentration enhancing interfacial adsorption and inhibiting bubble coalescence). In terms of types, AOS (Figure 9a) shows the most significant left shift of the particle size distribution peak (with the peak center at about 100 nm at 0.5 CMC) because the negatively charged groups enhance the electrostatic repulsion at the gas–liquid interface. CTAB (Figure 9b) causes the particle size distribution peak to shift slightly to larger sizes at low concentrations due to charge neutralization, and only inhibits coalescence through steric hindrance from dense molecular adsorption at high concentrations (>0.5 CMC). Nonionic APG-1214 (Figure 9c) and NP40 (Figure 9d) inhibit coalescence by relying on the steric hindrance effect of 5–8 nm hydration layers formed by hydrophilic groups. Their refining effect is better than that of CTAB but slightly inferior to that of AOS, and the peak shapes and variation trends of their particle size distributions are similar, reflecting a consistent nonionic stabilization mechanism.

Figure 10 presents the effects of surfactants with different types (anionic AOS, cationic CTAB, nonionic APG/NP40) and concentrations on the average particle size and zeta potential of CO_2 bubbles. However, the current way of connecting data points continuously is misleading (as different surfactants belong to independent systems rather than continuous concentration changes of the same system). In the follow-up, it will be optimized to subfigures (plotting by surfactant type, respectively) or grouped scatter plots to improve the clarity of data presentation. In terms of the trends, as the concentration of anionic AOS increases, the negative charge at the gas–liquid interface (the absolute value of the negative zeta potential) gradually enhances, and the bubbles continuously refine due to electrostatic repulsion (decreasing from 420 nm to 140 nm). The zeta potential of cationic CTAB gradually reverses from negative to positive with increasing concentration, and at low concentrations, the electrostatic stabilization ability may be weakened due to charge neutralization, resulting in local coalescence of bubbles (with the particle size showing an increasing trend at low

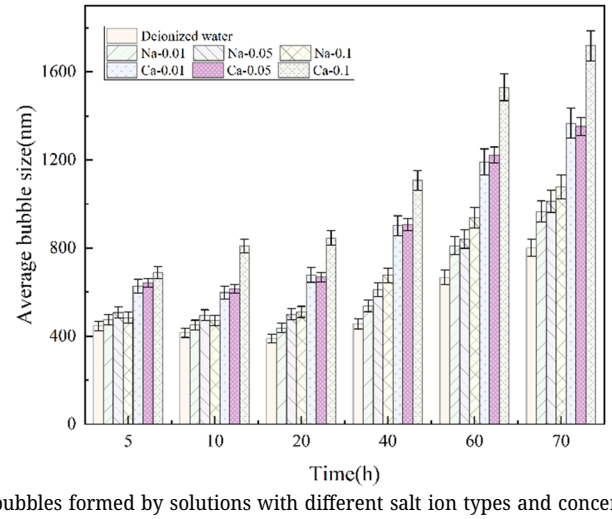

Figure 8. Changes in CO_2 nano bubbles formed by solutions with different salt ion types and concentrations over time.

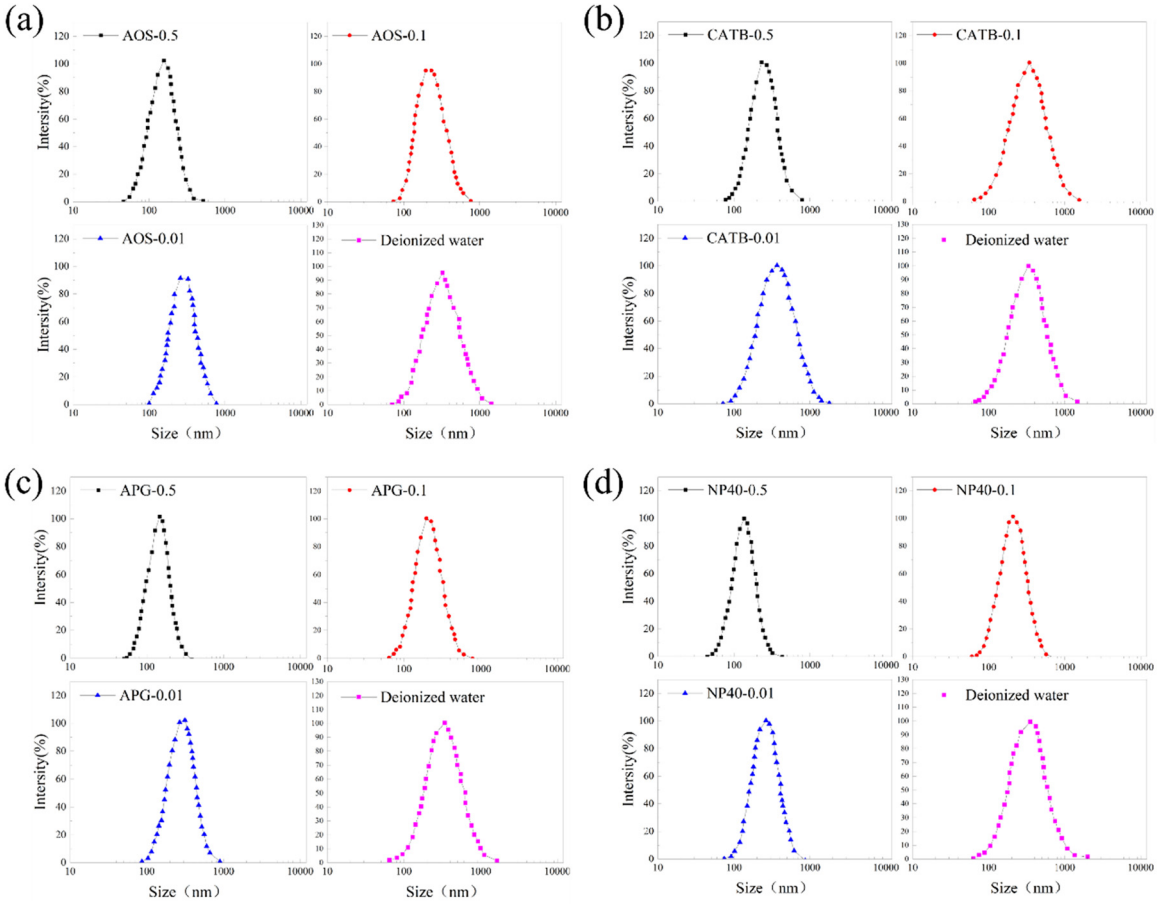

Figure 9. The influence of surfactant type and concentration on the formation of CO_2 nano bubbles. (a) Effect of AOS concentration; (b) effect of CATB concentration; (c) effect of APG concentration; (d) effect of NP40 concentration.

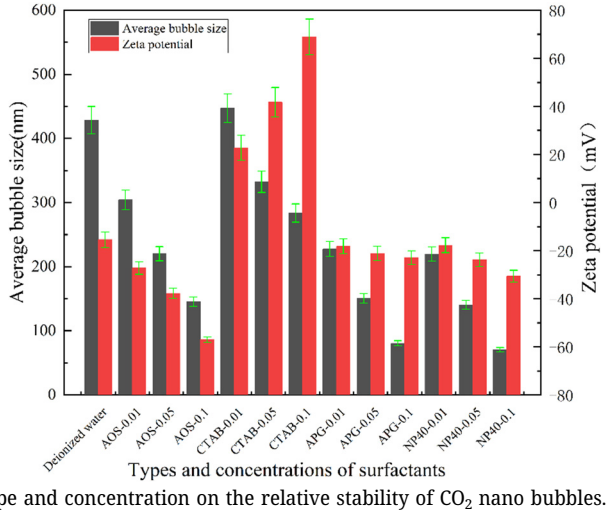

Figure 10. Effect of surfactant type and concentration on the relative stability of CO_2 nano bubbles.

concentrations). The zeta potentials of nonionic APG and NP40 fluctuate slightly in the range of −20~0 mV, and the bubbles rapidly refine to around 80 nm and remain stable. The similarity in their effects on nanobubbles arises because both rely on the hydration layers formed by hydrophilic groups to generate steric hindrance for inhibiting bubble coalescence, and the stabilization mechanism dominated by steric hindrance at the molecular level is consistent.

Figure 11 illustrates the time evolution of the average particle size of CO_2 bubbles in deionized water and surfactant solutions with different types and concentrations. The bubble size in deionized water increases continuously over time, consistent with the coarsening feature driven by Ostwald ripening. After adding surfactants, the growth of particle size is inhibited, and there is a dependence on both surfactant type and concentration. The higher the concentration of anionic AOS (0.01–0.5%), the slower the particle size growth, which is presumed to relate to the electrostatic repulsion caused by the enhanced interfacial negative charge. For cationic CTAB, the particle size grows faster initially at a low concentration (0.01%), possibly because charge neutralization weakens electrostatic stabilization, while the inhibition effect rebounds at high concentrations (the mechanism may involve micellar interfacial adsorption). Nonionic surfactants (APG, NP40) can significantly delay particle size growth even at a low concentration (0.1%), with smaller fluctuations within 70 h compared to ionic systems. It is inferred that the steric hindrance generated by the hydration layer formed by their molecules at the gas–liquid interface is the core of stabilization, and the steady-state particle size is significantly smaller than that in anionic systems.

Figure 12 reveals the differences in the mechanisms by which surfactants stabilize CO_2 nano bubbles. In deionized water, bubbles are maintained stable by a negative charge layer (−20 mV) formed by surface OH^-. Ionic surfactants achieve relative stability through a dual action (reducing

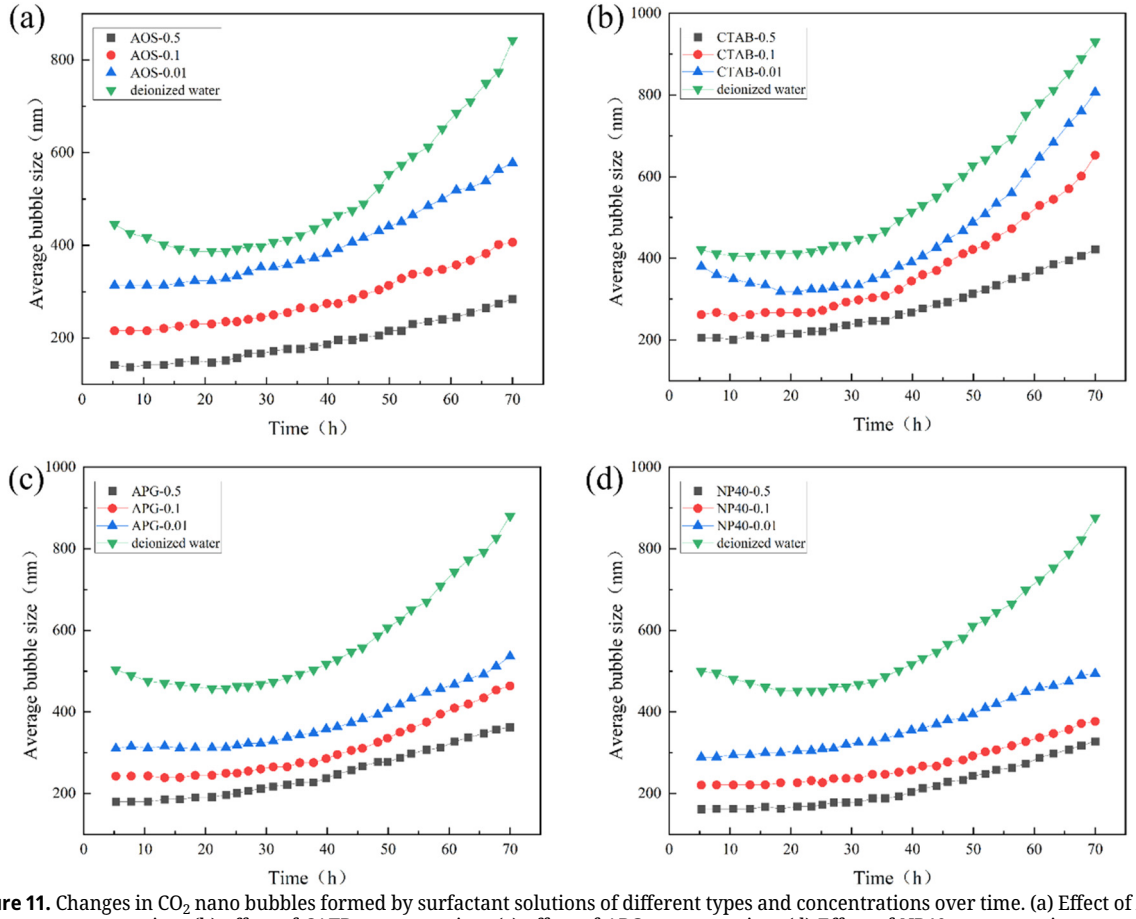

Figure 11. Changes in CO_2 nano bubbles formed by surfactant solutions of different types and concentrations over time. (a) Effect of AOS concentration; (b) effect of CATB concentration; (c) effect of APG concentration; (d) Effect of NP40 concentration.

surface tension to 30 mN/m, while regulating charge to −60 mV for anions and +56 mV for cations). Nonionic materials, on the other hand, generate entropy repulsion by forming a 5–8 nm thick hydration layer and retain some negative charges (−30 to −35 mV), exhibiting a unique spatial electrostatic synergistic stabilization mechanism.

3.3 CO_2 micro-nano system huff and puff experiment and oil displacement mechanism research

3.3.1 Assisted stimulation test of CO_2 micro-nano system

Imbibition experiments were conducted using CO_2, CO_2/LSW, and CO_2/LSW/surfactant solution, as shown in Figure 13.

The experiment compared the throughput and imbibition effects of three systems: pure CO_2, CO_2/low salinity water, and CO_2/low salinity water/surfactant. The experimental results show that the CO_2/low salinity water/surfactant composite system has the best oil displacement effect, with a recovery rate (43.6–52.5%) significantly higher than that of pure CO_2 (36.8%) and CO_2/low salinity water system (32.5%). Especially in the initial 30 h, the micro-nano dispersion system exhibits a faster oil recovery rate, and the concentration of surfactants is positively correlated with the recovery rate. This advantage stems from a triple synergistic effect: low salinity water improves wettability, surfactants reduce interfacial tension and form emulsions, and CO_2 promotes crude oil flow through dissolution, expansion, and extraction effects, collectively enhancing the imbibition throughput effect.

3.3.2 Analysis of factors affecting the CO_2 micro-nano dispersed system stimulation test

(1) The impact of injection pressure, gas–liquid ratio, and injection rate on the huff and puff effect

The experiment investigated the impact of different injection pressures (5 MPa, 10 MPa, 15 MPa, 20 MPa) on the stimulation effect of the CO_2/LSW-50/NP40 micro-nano dispersed system. By adjusting the CO_2 injection volume, the study explored the influence of various gas–liquid ratios on the stimulation effect of the CO_2/LSW-50/NP40 micro-nano dispersed system. Additionally, by adjusting the gas injection rate, the experiment examined its impact on the stimulation effect of the CO_2/LSW-50/NP40 micro-nano dispersed system.

Figure 14 shows that when the injection pressure of CO_2 exceeds 10 MPa, the oil recovery rate significantly increases, mainly due to the synergistic effect of high

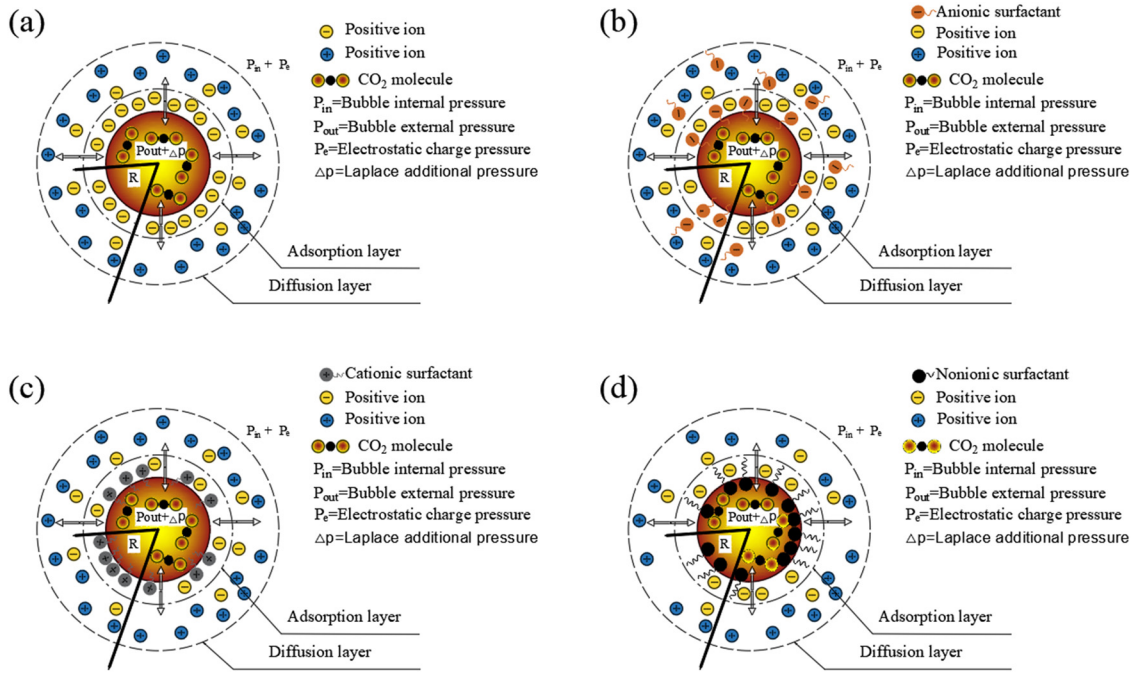

Figure 12. Schematic diagram of the mechanism by which ionic and nonionic surfactants stabilize CO_2 nano bubbles. (a) Effect of AOS concentration; (b) effect of CATB concentration; (c) Effect of APG concentration; (d) effect of NP40 concentration.

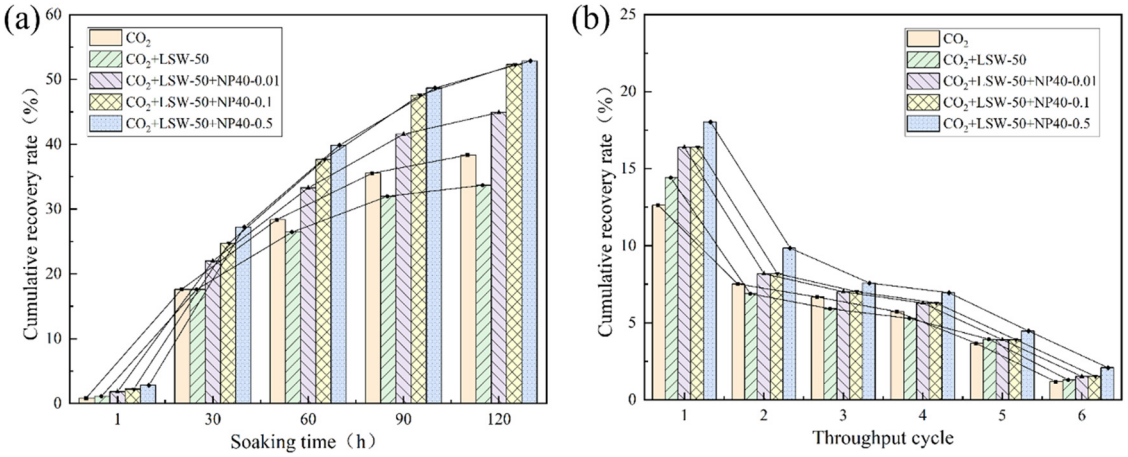

Figure 13. Oil recovery effect using CO_2 and different CO_2 micro-nano dispersion systems for huff and puff. (a) Effect of soaking time; (b) effect of throughput cycle.

pressure promoting CO_2 dissolution and diffusion, and low salinity water/surfactant. The optimal recovery rate is achieved when the gas–liquid ratio is 2:1, and the effect of excessive CO_2 injection is limited. Increasing the gas injection rate can increase the concentration of micro-nano bubbles, expand the contact area, promote the adsorption of surfactants and the transformation of rock wettability, thereby significantly improving the recovery rate. Comprehensive optimization of injection parameters (pressure >10 MPa, gas–liquid ratio of 2:1, higher injection rate) can maximize the oil displacement efficiency of CO_2 micro-nano dispersion system.

3.3.3 Oil displacement mechanism of CO_2 micro-nano system

The complete huff-and-puff oil recovery mechanism of the CO_2/LSW/surfactant micro-nano dispersion system is as follows: In the high-pressure injection stage, the system moves rapidly, relying on the fracture network characteristics of shale reservoirs, laying a spatial foundation for subsequent processes. After entering the soaking period, it undergoes three key stages of action in sequence (Figure 15). During the initial stage, micro-nano bubbles burst to release active components, which, combined with the wettability

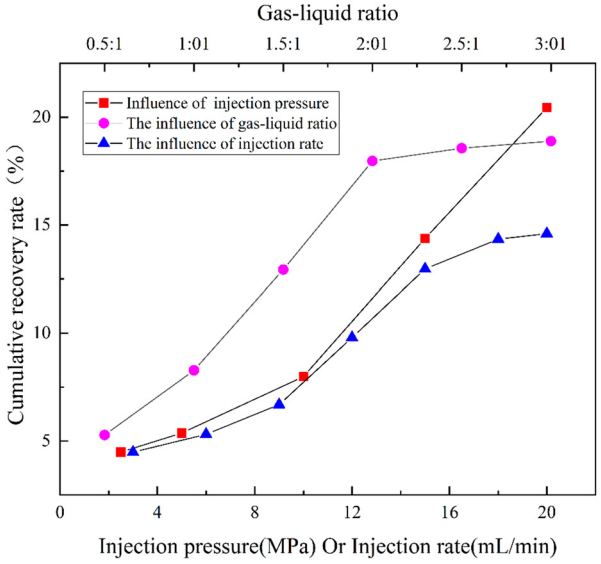

Figure 14. The influence of injection pressure, gas–liquid ratio, and injection rate on the effectiveness of huff and puff oil recovery.

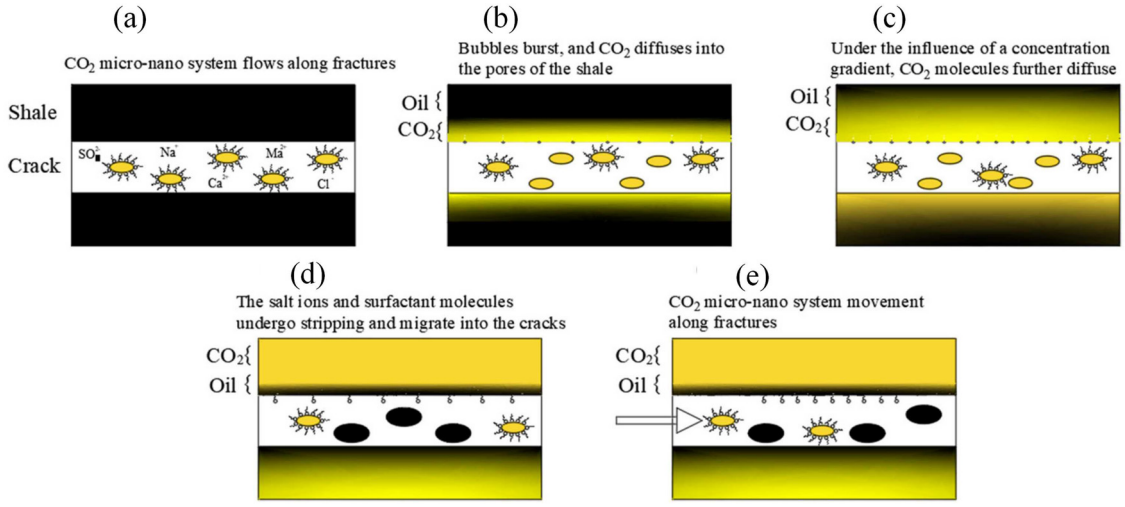

Figure 15. Schematic diagram of the CO_2 micro-nano dispersed system stimulation process. (a) Dispersion injection; (b) soaking; (c) diffusion; (d) ion migration; (e) oil displacement.

regulation effect, promote the wettability alteration of the matrix surface and improve the contact condition between crude oil and the system. In the middle stage, CO_2 realizes crude oil viscosity reduction and light component extraction by virtue of its molecular diffusion property, while surfactants and LSW synergistically exert the imbibition displacement effect to enhance the stripping driving force between crude oil and pore matrix. In the later stage, under the synergistic action of the above multiple mechanisms, crude oil continuously detaches from nano-pores. Finally, entering the flowback stage, the activated crude oil converges along the fracture network to the wellbore for production. This process innovatively integrates the dual advantages of physical driving forces (CO_2 diffusion, bubble movement) and chemical imbibition (wettability alteration, imbibition displacement). It not only specifically addresses the defect of easy channeling along fractures in single CO_2 flooding, but also significantly improves the oil production efficiency in the matrix through the synergy of multiple mechanisms.

4. Conclusion

(1) The particle size distribution and relative stability of CO_2 micro-nano dispersed systems are significantly influenced by standing time, temperature, pH value, and flow conditions. Among these factors, an alkaline environment and moderate temperature increase contribute to enhancing bubble relative stability.

(2) Inorganic salts and surfactants play a crucial role in regulating the size and relative stability of CO_2 nano bubbles. Divalent ions (such as Ca^{2+}) accelerate bubble coarsening, while anionic and nonionic surfactants (such as AOS, APG-1214) significantly enhance bubble relative stability through electrostatic repulsion or steric hindrance mechanisms.

(3) The CO_2/LSW/surfactant composite system exhibits excellent oil displacement performance in huff and puff experiments, with a recovery rate increased by more than 10% compared to single CO_2 injection. Its mechanism combines multiple advantages such as the dissolution and diffusion of CO_2, the imbibition effect of LSW, and the wettability regulation of surfactants.

(4) Injection pressure (>10 MPa), gas–liquid ratio (2:1), and a higher gas injection rate are key parameters for optimizing oil displacement efficiency, effectively expanding the contact area between CO_2 and shale, and suppressing gas channeling.

(5) This technology provides an innovative solution for the efficient development of shale oil reservoirs, with the dual potential of enhancing oil recovery and CO_2 sequestration. In the future, its feasibility for industrial-scale application can be further explored.

Funding information

This research did not receive any specific grant from funding agencies in the public, commercial, or not-for-profit sectors.

Author contributions

Tao Zhang: Methodology, investigation, and writing – original draft Preparation. Bengang Li: Investigation and

writing – original draft preparation. Baoche Liu: Investigation and writing – review and editing. Tenghuan Zhang: Formal analysis and writing – review and editing. Jianke Ren: Data curation and writing – review and editing. Chunmei Xu: Writing – review and editing. Shijun Chen: Conceptualization and writing – review and editing.

Conflict of interest statement

There is no conflict of interest.

Data availability statement

The original contributions presented in this study are included in the article material. Further inquiries can be directed to the corresponding author(s).

References

[1] Jiang, Z., Zhang, W., Liang, C., Wang, Y., Liu, H., Chen, X., Basic characteristics and evaluation of shale oil reservoirs, Petrol. Res., 2016; 1(2): 149–163. doi: 10.1016/S2096-2495(17)30039-X.

[2] Li, S., Zhang, S., Zou, Y., Zhang, X., Ma, X., Wu, S., et al., Experimental study on the feasibility of supercritical CO_2-gel fracturing for stimulating shale oil reservoirs, Eng. Fract. Mech., 2020; 238: 107276. doi: 10.1016/j.engfracmech.2020.107276.

[3] Fu, L., Shao, Y., Shao, M., Zhu, T., Li, X., Yang, Z., et al., Application and research progress of CO_2 stimulation technology in unconventional oil and gas reservoirs: A review and prospect, Energy Fuels, 2023; 37(24): 19400–19418. doi: 10.1021/acs.energyfuels.3c02945.

[4] Tu, J., Sheng, J., Experimental and numerical study of surfactant solution spontaneous imbibition in shale oil reservoirs, J. Taiwan Inst. Chem. E., 2020; 106: 169–182. doi: 10.1016/j.jtice.2019.11.003.

[5] Di, Z., Wang, Y., Chang, C., Song, H., Lu, X., Cheng, F., Synergistic gas-slag scheme to mitigate CO_2 emissions from the steel industry, Nat. Sustain., 2025; 1–10: doi: 10.1038/s41893-025-01572-2.

[6] Hazra, B., Vishal, V., Sethi, C., Chandra, D. (2022). Impact of supercritical CO_2 on shale reservoirs and its implication for CO_2 sequestration, Energy Fuels, 36(17), 9882–9903. doi: 10.1021/acs.energyfuels.2c01894.

[7] Yu, H., Xu, H., Fu, W., Lu, X., Chen, Z., Qi, S., et al., Extraction of shale oil with supercritical CO_2: Effects of number of fractures and injection pressure, Fuel, 2021; 285: 118977. doi: 10.1016/j.fuel.2020.118977.

[8] Hu, Y., Hao, M., Chen, G., Sun, R., Li, S., Technologies and practice of CO_2 flooding and sequestration in China, Petrol. Explor. Dev., 2019; 46(4): 753–766. doi: 10.1016/S1876-3804(19)60233-8.

[9] Pan, X., Sun, L., Liu, Q., Huo, X., Chen, F., Wang, Y., et al., Mechanism of CO_2 flooding in shale reservoirs-insights from nanofluids, Nanoscale, 2025; 17(3): 1524–1535. doi: 10.1039/D4NR02474E.

[10] Xia, D., Yang, Z., Gao, T., Li, H., Lin, W., Characteristics of micro- and nano-pores in shale oil reservoirs, J. Petrol. Explor. Prod. Te., 2021; 11(1): 157–169. doi: 10.1007/s13202-020-01012-1.

[11] Zhu, H., Ju, Y., Lu, W., Han, K., Qi, Y., Neupane, B., Sun, Y., Cai, J., Xu, T., Huang, C., Han, Y., The characteristics and evolution of micro-nano scale pores in shales and coals, J. Nanosci. Nanotechno., 2017; 17(9): 6124–6138. doi: 10.1166/jnn.2017.14529.

[12] Lv, Q., Hou, J., Chen, J., Ji, Y., Cheng, Z., Lv, J., et al., Experimental study on elastic development characteristics and imbibition mechanism of shale oil reservoirs at micro-nano scale, Fuel, 2025; 381: 133557. doi: 10.1016/j.fuel.2024.133557.

[13] Xue, Z., Nishio, S., Hagiwara, N., Matsuoka, T., Microbubble carbon dioxide injection for enhanced dissolution in geological sequestration and improved oil recovery, Energy Procedia, 2014; 63: 7939–7946. doi: 10.1016/j.egypro.2014.11.828.

[14] Guo, C., Zhang, L., Zhang, Q., Ni, C., Deng, N., Huang, X., Efficient adsorptive removal of phosphonate antiscalant HEDP by Mg-Al LDH, Separations, 2025; 12: 259. doi: 10.3390/separations12100259.

[15] Jadhav, A., Barigou, M., On the clustering of bulk nanobubbles and their colloidal relative stability, J. Colloid Interf. Sci., 2021; 601: 816–824. doi: 10.1016/j.jcis.2021.05.154.

[16] Zhou, S., Nazari, S., Hassanzadeh, A., Bu, X., Ni, C., Peng, Y., et al., The effect of preparation time and aeration rate on the properties of bulk micro-nano bubble water using hydrodynamic cavitation, Ultrason. Sonochem., 2022; 84: 105965. doi: 10.1016/j.ultsonch.2022.105965.

[17] Rong, L., Zhang, B., Qiu, H., Zhang, H., Yu, J., Yuan, Q., et al., Significant generational effects of tetracyclines upon the promoting plasmid-mediated conjugative transfer between typical wastewater bacteria and its mechanisms, Water Res., 2025; 287: 124290. doi: 10.1016/j.watres.2025.124290.

[18] Nirmalkar, N., Pacek, A., Barigou, M., On the existence and relative stability of bulk nanobubbles,

Langmuir, 2018; 34(37): 10964–10973. doi: 10.1021/acs.langmuir.8b01163.

[19] Oh, S., Kim, J., Generation and relative stability of bulk nanobubbles, Langmuir, 2017; 33(15): 3818–3823. doi: 10.1021/acs.langmuir.7b00510.

[20] Guo, C., Xu, Y., Deng, N., Huang, X., Efficient degradation of organophosphorus pesticides and in situ phosphate recovery via NiFe-LDH activated peroxymonosulfate, Chem. Eng. J., 2025; 524: 169107. doi: 10.1016/j.cej.2025.169107.

[21] Kukizaki, M., Goto, M., Size control of nanobubbles generated from Shirasu-porous-glass (SPG) membranes, J.Membrane Sci., 2006; 281(1–2): 386–396. doi: 10.1016/j.memsci.2006.04.007.

[22] Meng, T., Liu, R., Cai, J., Cheng, X., He, Z., Zhao, Z., Breaking structural symmetry of atomically dispersed Co sites for boosting oxygen reduction. Adv. Funct. Mater., 2025; 36(17): e22046. doi: 10.1002/adfm.202522046.

[23] Li, J., Wen, M., Yang, J., Liu, Y., Jiang, Z., Chen, J., Synthesis and analysis of magnetic nanoparticles within foam matrix for foam drainage gas production, Geo. Sci. Eng., 2024; 238: 212887. doi: 10.1016/j.geoen.2024.212887.

[24] Zhang, Q., Xu, B., Ni, C., Huang, X. (2026). Synergistic Dual-Heteroatom Engineering Enables pH-universal Ammonia Electrosynthesis in a Solid Electrolyte Reactor, Appl. Catal. B Environ., 127153. doi: 10.1016/j.apcatb.2026.127153.

[25] Li, M., Ma, X., Eisener, J., Pfeiffer, P., Ohl, C., Sun, C., How bulk nanobubbles are stable over a wide range of temperatures, J. Colloid Interf. Sci., 2021; 596: 184–198. doi: 10.1016/j.jcis.2021.03.064.

[26] Pan, X., Zhao, Z., Huang, X., Deng, N., (2026). Carboxyl-Fe and phosphonate-Fe interactions control the redistribution of organic phosphate during ferrihydrite transformation, Chem. Geol, 720, 123597. doi: 10.1016/j.chemgeo.2026.123597.

[27] Jadhav, A., Barigou, M., On the clustering of bulk nanobubbles and their colloidal relative stability, J. Colloid Interf. Sci., 2021; 601: 816–824. doi: 10.1016/j.jcis.2021.05.154.